Interfacial Properties of N_{TAIL}, an Intrinsically Disordered Protein

Anaïs Bénarouche,[1,2] Johnny Habchi,[3] Alain Cagna,[2] Ofelia Maniti,[4] Agnès Girard-Egrot,[4] Jean-François Cavalier,[1] Sonia Longhi,[3,*] and Frédéric Carrière[1,*]

[1]Aix-Marseille University, CNRS, Enzymologie Interfaciale et Physiologie de la Lipolyse UMR 7282, Marseille, France; [2]TECLIS Scientific, Tassin, France; [3]Aix-Marseille University, CNRS, Architecture et Fonction des Macromolécules Biologiques (AFMB) UMR 7257, Marseille, France; and [4]Université de Lyon, Université Claude Bernard Lyon 1, CNRS, INSA Lyon, CPE Lyon, UMR 5246 Institut de Chimie et Biochimie Moléculaires et Supramoléculaires, Equipe Génie Enzymatique, Membranes Biomimétiques et Assemblages Supramoléculaires (GEMBAS), Villeurbanne, France

ABSTRACT Intrinsically disordered proteins (IDPs) lack stable secondary and tertiary structure under physiological conditions in the absence of their biological partners and thus exist as dynamic ensembles of interconverting conformers, often highly soluble in water. However, in some cases, IDPs such as the ones involved in neurodegenerative diseases can form protein aggregates and their aggregation process may be triggered by the interaction with membranes. Although the interfacial behavior of globular proteins has been extensively studied, experimental data on IDPs at the air/water (A/W) and water/lipid interfaces are scarce. We studied here the intrinsically disordered C-terminal domain of the Hendra virus nucleoprotein (N_{TAIL}) and compared its interfacial properties to those of lysozyme that is taken as a model globular protein of similar molecular mass. Adsorption of N_{TAIL} at the A/W interface was studied in the absence and presence of phospholipids using Langmuir films, polarization modulated-infrared reflection-absorption spectroscopy, and an automated drop tensiometer for interfacial tension and elastic modulus determination with oscillating bubbles. N_{TAIL} showed a significant surface activity, with a higher adsorption capacity at the A/W interface and penetration into egg phosphatidylcholine monolayer compared to lysozyme. Whereas lysozyme remains folded upon compression of the protein layer at the A/W interface and shows a quasi-pure elastic behavior, N_{TAIL} shows a much higher molecular area and forms a highly viscoelastic film with a high dilational modulus. To our knowledge, a new disorder-to-order transition is thus observed for the N_{TAIL} protein that folds into an antiparallel β-sheet at the A/W interface and presents strong intermolecular interactions.

INTRODUCTION

Proteins are major components of the living cell where they play crucial structural and functional roles, and their dysfunctions can lead to various pathologies. These dysfunctions are often associated with gene mutations leading to inactive or noncorrectly folded proteins/enzymes. This usually applies to globular proteins with well-defined 3D structure and function(s) associated with this structure. With the increasing evidence that intrinsically disordered proteins (IDPs) or intrinsically disordered protein regions are highly represented among proteins (1), new concepts have emerged to describe and possibly explain some protein misfolding disorders such as neurodegenerative diseases. Indeed, the aggregation of IDPs into amyloid fibrils is directly associated with the onset and progression of these pathological disorders. For instance, Alzheimer's and Parkinson's diseases are tightly associated with the aggregation of otherwise soluble IDPs that form protein deposits in the brain of patients and lead to neuronal death (2–6). In that context, it is important to better understand the key factors that can trigger the folding and aggregation of IDPs.

IDPs are functional proteins that are devoid of stable secondary and tertiary structure under physiological conditions of pH and salinity in the absence of a partner/ligand (7–10). They thus exist as dynamic ensembles of interconverting conformers and differ from structured globular proteins at several levels, including amino acid composition, sequence complexity, hydropathy, charge, and flexibility. IDPs are typically depleted in bulky and hydrophobic residues (W, C, F, Y, I, L, V, and N), also called "order-promoting residues", and are conversely enriched in polar and charged residues (A, R, G, Q, S, P, E, and K), also called "disorder-promoting residues" (8). These peculiar properties dictate the behavior of IDPs in various environments and they have been used for the development of protein disorder predictors (11,12). Because of their enrichment in polar/charged

*Correspondence: sonia.longhi@afmb.univ-mrs.fr or carriere@imm.cnrs.fr

residues, IDPs are characterized by a hydration significantly higher than that of ordered proteins (13). As such, IDPs can reasonably be expected to exhibit a distinct behavior not only in bulk but also at air/water (A/W) and lipid/water interfaces. This is for instance the case for the α-synuclein protein, the aggregation of which is involved in the neuropathology of Parkinson's disease. α-synuclein is an IDP in its monomeric form in the aqueous phase, but it is known to form a stable monolayer at the A/W (14) and lipid/water (phospholipids vesicles) (15) interfaces although adopting a partial α-helical conformation (16,17). Infrared reflection-absorption spectroscopy (IRRAS) at the A/W interface suggests that the helical axis is parallel to the interface plane (14). On the other hand, depending on the lipid-to-protein ratio and the nature of lipids, α-synuclein can adopt a β-sheet conformation that further aggregates into amyloid fibrils; these are the major component of Lewis bodies that are formed inside dopaminergic cells, a hallmark of Parkinson's disease patients (2–4). In the case of the amyloid-β protein (Aβ), an IDP involved in Alzheimer's disease, it was found that this peptide accumulates at the A/W interface predominantly in an α-helical conformation (5). Contrary to α-synuclein, the intrinsically disordered amyloid-β peptide undergoes a disorder to α-helix transition before its adsorption at the interface (5). The protein tau, another IDP involved in the Alzheimer's disease, is able to strongly interact with the A/W interface, intercalates into negatively charged lipid monolayers and bilayers, and induces membrane morphological changes and disruption (6). This protein-lipid interaction induces a partial and more compact conformation with a density similar to that of a folded protein.

The need for more information on the interfacial behavior of IDPs and comparison with globular proteins prompted us to investigate the interfacial properties of a model IDP, the intrinsically disordered C-terminal domain of the Hendra virus (HeV) nucleoprotein (N_{TAIL}), a protein responsible for the encapsidation of the viral genome (18,19). HeV N_{TAIL} is a disordered protein domain of 140 residues and 15.3 kDa that has been well characterized by various biophysical approaches (20–22). In this study, we compared the behavior of HeV N_{TAIL} at the air-water interface, in the absence and presence of phospholipids, with that of lysozyme using Langmuir films, polarization modulated-infrared reflection-absorption spectroscopy (PM-IRRAS), and a dynamic drop tensiometer. Lysozyme served as a model of folded globular protein having a molecular mass (14.3 kDa) close to that of HeV N_{TAIL}.

MATERIALS AND METHODS

Reagents

Egg phosphatidylcholine (EggPC) from Avanti Polar Lipids (Alabaster, AL) was purchased from Coger (Paris, France) and was >99% purity. All other chemicals (NaCl, $CaCl_2$, Tris, and EDTA) were purchased from Sigma-Aldrich (St. Quentin-Fallavier, France) and were BioXtra grade ($\geq$99.0% purity). Chloroform (anhydrous for analysis, stabilized with amylene) was purchased from Carlo Erba Reactifs-SDS (Val de Reuil, France).

Proteins

In this study, we used the HeV N_{TAIL} F527W variant bearing a phenylalanine to tryptophan substitution at position 527. This variant was previously shown to exhibit a behavior very close to that of the wild-type protein in terms of hydrodynamic and spectroscopic properties, as well as interaction with its physiological partner (23). A construct encoding residues 400–532 of the Hendra virus nucleoprotein N and a hexahistidine tag fused to the N-terminal end of the protein was used for expression in *E. coli* Rosetta [DE3] pLysS strain (Novagen/Merck Millipore, Burlington, MA), as described previously (23). Protein purification was carried out according to (23) and a stock solution of purified N_{TAIL} (11.5 mg mL^{-1}; 750 μM) in 10 mM sodium phosphate pH 7, NaCl 150 mM was prepared. A diluted solution of 0.56 mg mL^{-1} N_{TAIL} (36 μM) was used for monolayer studies. Lysozyme from chicken egg white ($\geq$90% purity) was purchased from Sigma-Aldrich (Cat. No. L6876) and a stock solution of 0.34 mg mL^{-1} (24 μM) was prepared in Milli-Q water (Millipore, Billerica, MA). Proteins concentrations in their respective stock solutions were determined by amino acid analysis performed at the Laboratoire d'Enzymologie Moléculaire, Institut de Biologie Structurale (Grenoble, France).

Protein analysis

Protein sequence analyses were performed using the HeV N_{TAIL} sequence reported in (20), with the exception of the F527W substitution, and chicken egg white lysozyme sequence (NCBI Reference Sequence: NP_990612.1; UniProt: P00698). Hydrophobic cluster analysis (HCA) was performed using the HCA 1.0.2 program available at http://mobyle.rpbs.univ-paris-diderot.fr/cgi-bin/portal.py#forms::HCA (24).

Far-UV circular dichroism (CD) spectra of HeV N_{TAIL} and lysozyme were recorded on a model No. 810 Dichrograph (Jasco, Oklahoma City, OK) using 1-mm-thick quartz cells and protein solutions at 0.1 mg/mL in 10 mM sodium phosphate pH 7 at 20°C. CD spectra were measured between 185 and 260 nm at 0.2 nm min^{-1} and were averaged from three independent acquisitions. Protein content in secondary structure was estimated from CD spectrum analysis using the DICROWEB server (25,26).

Monomolecular films: general methodology

All experiments were performed at room temperature (25°C) using homemade Teflon (Chemours, Wilmington, DC) troughs and the KSV5000 barostat equipment (KSV Instruments, Helsinki, Finland) equipped with a temperature sensor probe, a Langmuir film balance, and a mobile barrier for compression isotherm experiments. The principle of this method was previously described (27,28). Surface pressure (measured using a Wilhelmy plate, perimeter 3.924 cm), temperature, and barrier movement were monitored by the KSV Device Server Software v.3.50 (KSV Instruments) running under Windows 7. Before each experiment, the Teflon troughs were cleaned with tap water, then gently brushed in the presence of distilled ethanol, before being washed again with tap water and abundantly rinsed with Milli-Q water. Residual surface-active impurities were removed before each experiment by simultaneous sweeping and suction of the surface (29). For all experiments, the aqueous subphase was composed of Tris/HCl Buffer (10 mM Tris/HCl, 100 mM NaCl, 21 mM $CaCl_2$, 1 mM EDTA) at pH 7.0 prepared with Milli-Q water. The phospholipid monolayer was prepared by spreading a few microliters of an eggPC solution (1 mg mL^{-1} in chloroform) until the desired initial surface pressure (Π_i) was reached. The waiting time for solvent evaporation and for the film to reach equilibrium varied from 10 to 20 min, depending on the spreading volume and the initial surface pressure.

Surface pressure-area isotherms

Cycles of compression–decompression isotherms were performed at a speed of 5 mm min^{-1} (3.05 cm^2 min^{-1}), with hold times of 60 min between each compression/decompression cycle. The protein monolayer was formed by spreading 10 or 50 μL of N_{TAIL} (0.56 mg mL^{-1}) or lysozyme (0.34 mg mL^{-1}), respectively, over the surface of a rectangular Teflon trough (volume 126.3 mL; surface area, 210.5 cm^2). After stabilization of the monolayer for at least 20 min, the film compression was started and the increase in surface pressure was recorded. The apparent molecular area of the protein was deduced from the amount spread at the surface of the trough and the area covered by the film. All compression-decompression isotherms were repeated ($n = 3$) with a coefficient of variation not exceeding 5%.

Protein adsorption onto eggPC monomolecular films at 25°C

The eggPC monomolecular film was formed over the surface of a home-made round Teflon trough (volume, 9.4 mL; surface area, 8.04 cm^2) by spreading an eggPC chloroform solution (1 mg mL^{-1}) until the desired initial surface pressure (Π_i) was reached. After injecting the proteins into the aqueous subphase with a Hamilton syringe (from 5.0 to 32 μL for N_{TAIL} or lysozyme stock solutions resulting in final concentrations ranging from 8.4 to 60 nM, respectively), the surface pressure increase due to the adsorption/penetration of the protein onto the eggPC monolayer was continuously recorded (every 5 s) until the equilibrium surface pressure (Π_e) was reached. The aqueous subphase, composed of the same Tris/HCl buffer (pH 7.0) as described above, was continuously stirred with a 1 cm magnetic bar rotating at 250 rpm.

Treatment of kinetic data of protein adsorption onto eggPC monolayer

To compare and analyze the adsorption step of N_{TAIL} and lysozyme, apparent kinetic parameters of adsorption (k_a, M^{-1} s^{-1}) and desorption (k_d, s^{-1}) onto the eggPC films were calculated according to (28,30). Briefly, the Langmuir adsorption isotherm equation adapted to surface pressure measurements (Eq. 1) was used to fit the experimental data (i.e., surface pressure increase ($\Delta\Pi$) with time):

$$\Pi(t) = \Pi_i + \Delta\Pi_{max}.\theta.[1-\exp(\sigma \cdot t)], \quad (1)$$

where $\Pi(t)$ is the surface pressure measured as a function of time; Π_i is the initial surface pressure; $\Delta\Pi_{max}$ is the maximum variation of surface pressure reached upon binding of the protein; θ is the fraction of the total free adsorption (binding) sites coverage; and $\sigma = (k_a.C_{E0} + k_d)$ with C_{E0} (mol L^{-1}) being the protein concentration in the subphase of the trough.

Fitting the experimental data points to Eq. 1 using KaleidaGraph 4.1 software (Synergy; http://kaleidagraph.software.informer.com/4.1/) allowed calculating σ-values for multiple C_{E0} concentrations at each Π_i investigated. Values of k_a and k_d were then determined from the slope and y intercept, respectively, of the linear plot of σ versus C_{E0}. The adsorption equilibrium coefficient, K_{Ads}, which represents the binding affinity between the protein and the lipid film, was obtained from the ratio of the measured rate constants ($K_{Ads} = k_a/k_d = 1/K_D$). Using the mathematical equations derived from the interfacial kinetic model of Panaiotov and Verger (31), it becomes possible to estimate, by indirect calculation, the theoretical value of protein interfacial concentration (Γ_E*, molecule cm^{-2}) based on Eq. 2, where S_{trough}/V_{trough} represents the surface area-volume ratio (cm^{-1}) of the reaction compartment of the Teflon trough:

$$\Gamma_{E*} = C_{E0} \Big/ \left[(1 + K_D) \cdot \left(\frac{S_{trough}}{V_{trough}}\right)\right]. \quad (2)$$

From Eq. 2, the molar fraction ($\Phi_{E*(\%)}$, mol %) of total protein that is adsorbed onto the lipid monolayer can then be deduced (Eq. 3):

$$\Phi_{E*(\%)} = \left[\Gamma_{E*} \cdot \left(\frac{S_{trough}}{V_{trough}}\right)\right] \Big/ C_{E0} = 100/(1 + K_D). \quad (3)$$

Finally, the mathematical expression of the molecular area (A_E*, $Å^2$ $molecule^{-1}$) occupied by the adsorbed protein onto eggPC films can be expressed as

$$A_{E*} = \left[\left(S_{trough} - A_{eggPC} \cdot n_{eggPC}\right) \cdot \theta\right] \Big/ \left(\Gamma_{E*} \cdot S_{trough}\right). \quad (4)$$

A_{eggPC} ($Å^2$ $molecule^{-1}$) is the molecular area of eggPC deduced from the surface pressure (Π)-molecular area isotherm at the final equilibrium surface pressure reached upon N_{TAIL} or lysozyme adsorption; n_{eggPC} is the number of eggPC molecules spread at the air/water interface at the working initial surface pressure (Π_i); and θ is the fractional surface coverage determined in Eq. 1.

PM-IRRAS measurements

A rectangular Teflon trough (volume, 52 mL; surface area, 90 cm^2; Nima Technology, Manchester, UK) was used to perform adsorption kinetics concomitantly with PM-IRRAS measurements at 25°C. The subphase was composed of the same Tris/HCl buffer (pH 7.0) as described above. After surface pressure stabilization, a volume of 85 μL of N_{TAIL} (36 μM) or 131 μL of lysozyme (24 μM) stock solution was injected into the subphase leading to a final bulk protein concentration of 60 nM. PM-IRRAS spectra were recorded either at the air/buffer interface or in the presence of an eggPC film spread at an initial surface pressure of 4 mN m^{-1}, which favored protein adsorption/penetration into the lipid layer.

PM-IRRAS analysis of N_{TAIL} adsorbed at the A/W interface in the presence and absence of an eggPC monolayer was performed as previously described (32–35). The spectra were recorded on a Nicolet Nexus 870 Fourier transform infrared spectrometer (Thermo Fisher Scientific, Madison, WI). The light beam was reflected toward the optical bench by a mobile mirror. It was then polarized by a ZnSe polarizer and directed toward a photoelastic modulator that modulated the beam between a parallel (p) and perpendicular (s) polarization. The light beam was directed toward the monolayer at an angle of 75° and reflected on a photovoltaic MCT-A detector cooled at 77 K. The detected signal was then processed to obtain the differential reflectivity spectrum (Eq. 5):

$$\Delta R/R = J_2 \times \left(R_p - R_s\right) \Big/ \left(R_p + R_s\right), \quad (5)$$

where J_2 is the Bessel function, which depends only on the photoelastic modulator; and R_s and R_p are the parallel and perpendicular reflectivities, respectively. To remove the Bessel function contribution, as well as that of water absorption, the monolayer spectrum was divided by that of the pure subphase. For each spectrum, 1024 scans were recorded at a resolution of 8 cm^{-1} and were summed up for pure N_{TAIL}, pure lipid monolayer, and lipid monolayer in the presence of N_{TAIL}. Due to low amounts of protein, spectra were acquired every 12 min and for 12 min after protein adsorption equilibrium was reached (5 h at the air-water interface and 2.3 h in the presence of eggPC). For each experiment, three series of scans were averaged.

Experiments with the dynamic drop tensiometer

All experiments were performed with a Tracker Drop Tensiometer (Teclis, Tassin, France) (36). A 4 μL air bubble was formed at the tip of a J-tube submerged in 4.5 mL of bulk buffer. The bulk buffer was 10 mM Tris/HCl (pH 7.0), 100 mM NaCl, and 21 mM $CaCl_2$. The profile of the bubble was collected by a high-speed CCD camera and surface tension (γ) was

estimated from the Laplace equation adapted for a bubble. This device allowed measuring changes in surface tension after injection of proteins (N_{TAIL} or lysozyme at 80 nM final concentration) or phospholipids (eggPC) in the bulk phase. In this latter case, 450 μL of eggPC large unilamellar vesicles (LUV; 0.5% w/v) were injected in the bulk phase (0.05% w/v final concentration) for deposition of phospholipids at the air/water interface upon LUV adsorption at the surface of the air bubble. LUVs were prepared by extrusion through a 100-nm cutoff membrane using a Mini-Extruder (Avanti Polar Lipids) and their size distribution was checked by dynamic light scattering using a Zetasizer Nano S (Malvern Instruments, Malvern, United Kingdom).

For surface rheometry measurements, the air bubble was subjected to sinusoidal variations of its volume at a frequency of 0.2 Hz to produce the sinusoidal area variations required for measurement of the surface dilational modulus E and its elastic (E') and viscous (E'') components as a function of the imposed frequency. The amplitude of the relative area variation was $\Delta A/A = 0.25$. All measurements were carried out at 25°C.

Variations in the surface dilational modulus E as a function of surface pressure Π were fitted using a 2D solution treatment. Surface pressure is given by a first-order surface equation of state based on Frumkin-Lucassen's isotherm and including terms for entropy and enthalpy of surface mixing of solvent and surfactant with nonequal molecular area (37):

$$\Pi = \frac{RT}{\omega_1}\left[-\ln\left(1-\frac{\Gamma}{\Gamma_{inf}}\right)-\left(1-\frac{1}{S}\right)\frac{\Gamma}{\Gamma_{inf}} - \frac{H}{RT}\left(\frac{\Gamma}{\Gamma_{inf}}\right)^2\right] \quad (6)$$

in which ω_1 is the molecular area of the solvent (water), S is a size factor defined as the ratio of the molecular area of surfactant or solute (protein or eggPC in this study) to that of the solvent, H is the molar enthalpy of mixing at infinite dilution, Γ is the surface concentration of surfactant, Γ_{inf} is the maximum or saturation surface concentration of surfactant, R is the ideal gas constant, and T is the temperature. The dilational modulus E is given by the following equation (37,38):

$$E = \frac{RT}{\omega_1}\left[\frac{\frac{\Gamma}{\Gamma_{inf}}}{1-\frac{\Gamma}{\Gamma_{inf}}} - \left(1-\frac{1}{S}\right)\frac{\Gamma}{\Gamma_{inf}} - \frac{2H}{RT}\left(\frac{\Gamma}{\Gamma_{inf}}\right)^2\right]. \quad (7)$$

TABLE 1 Amino Acid Composition and Other Characteristic Parameters of N_{TAIL} and Lysozyme

Parameters	Hendra Virus N_{TAIL} F527W	Chicken Egg White Lysozyme
Size (amino acids)	140	129
Molecular mass (Da)	15,280.6	14,314.17
Stokes radius (Å) estimated by dynamic light scattering	28	19
Section (Å^2)	2463	1134
Isoelectric point	5.95	9.32
Amino Acids		
Ala (A)	12 (8.6%)	11 (8.5%)
Arg (R)	11 (7.9%)	11 (8.5%)
Asn (N)	8 (5.7%)	13 (10.1%)
Asp (D)	10 (7.1%)	7 (5.4%)
Cys (C)	0 (0.0%)	8 (6.2%)
Gln (Q)	8 (5.7%)	3 (2.3%)
Glu (E)	11 (7.9%)	2 (1.6%)
Gly (G)	10 (7.1%)	12 (9.3%)
His (H)	7 (5.0%)	1 (0.8%)
Ile (I)	3 (2.1%)	6 (4.7%)
Leu (L)	8 (5.7%)	8 (6.2%)
Lys (K)	6 (4.3%)	6 (4.7%)
Met (M)	4 (2.9%)	2 (1.6%)
Phe (F)	2 (1.4%)	3 (2.3%)
Pro (P)	7 (5.0%)	2 (1.6%)
Ser (S)	19 (13.6%)	11 (8.5%)
Thr (T)	5 (3.6%)	7 (5.4%)
Trp (W)	1 (0.7%)	6 (4.7%)
Tyr (Y)	0 (0.0%)	3 (2.3%)
Val (V)	8 (5.7%)	7 (5.4%)
Negatively charged	21 (15,0%)	9 (7.0%)
Positively charged	17 (12.1%)	17 (13.2%)
Hydrophobic	45 (32.1%)	45 (34.9%)
Semipolar	47 (33.6%)	43 (33.3%)
Aromatic	3 (2.1%)	12 (9.3%)
Aliphatic index	55.79	66.59
Secondary Structure Elements Deduced from CD Spectral Deconvolution		
α-Helices	5%	42%
β-Sheet	7%	26%
β-Turn	7%	9%
Coil	80%	22%

RESULTS

Structural comparison of N_{TAIL} and lysozyme in solution

Both N_{TAIL} and lysozyme have similar contents in terms of positively charged, hydrophobic, and semipolar amino acid residues, but mainly differ by their content in negatively charged (higher in N_{TAIL}) and aromatic (lower in N_{TAIL}) residues (Table 1). The HCA plots generated by hydrophobicity cluster analysis (24) show a depletion in hydrophobic clusters in N_{TAIL} compared to lysozyme (Fig. S1). The far-UV CD spectra of HeV N_{TAIL} (F570W variant) is typical of IDPs (Fig. 1), and its analysis reveals a very large proportion of random coils (80%) (Table 1), whereas the CD spectrum of lysozyme confirms a high content in regular secondary structure elements (40% α-helices, 12% β-sheets), in agreement with the known secondary (Fig. S1) and tertiary structure of lysozyme (PDB: 1LYZ (39)).

N_{TAIL} and lysozyme compression isotherms at the A/W interface

Langmuir films of N_{TAIL} and lysozyme were formed at the A/W interface and were then submitted to cycles of compression and decompression up to a final surface pressure of ~16 mN m^{-1} corresponding to the maximum penetration of N_{TAIL}. Some hysteresis of the surface pressure variation with molecular area was observed in both cases, but it was more pronounced with N_{TAIL} ($\Delta A = -118$ Å^2 at 2 mN m^{-1}; Fig. 2 *A*) than with lysozyme ($\Delta A = -17$ Å^2 at 2 mN m^{-1}; Fig. 2 *B*).

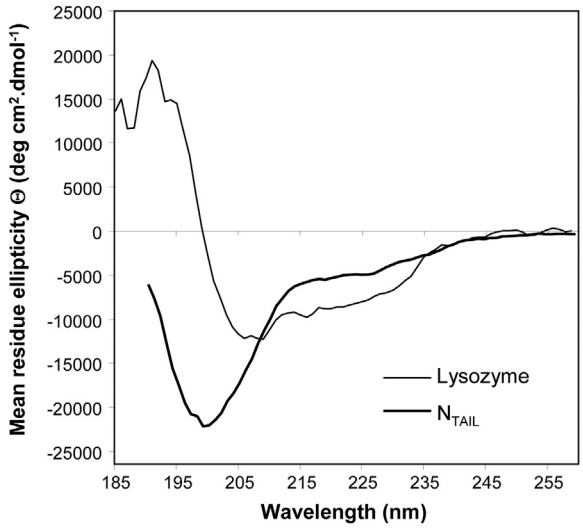


FIGURE 1 Far-UV circular dichroism spectra of HeV N_{TAIL} (F570W variant), and of lysozyme. Far-UV CD spectra were recorded using protein solutions at 0.1 mg mL^{-1} in 10 mM sodium phosphate pH 7 at 20°C.

The molecular areas occupied by the proteins at the A/W interface were extrapolated from the tangent at the inflection point of the compression curves. The average N_{TAIL} molecular area (A_{NTAIL}) was found to be 1868 ± 100 $Å^2$ ($n = 3$) and it was threefold larger than the molecular area estimated for lysozyme ($A_{Lysozyme} = 616 \pm 15$ $Å^2$; $n = 3$).

N_{TAIL} conformation and orientation at the air-water interface

The ability of N_{TAIL} molecules to form a layer at the A/W interface allowed us to investigate the protein conformation and orientation by PM-IRRAS. The PM-IRRAS spectrum of N_{TAIL} adsorbed at the A/W interface exhibits two main bands in the 1500–1700 cm^{-1} spectral region, assigned to the amide I and amide II vibrations (Fig. 3). This profile was rapidly observed after protein injection in the subphase and remained similar after protein adsorption equilibrium was reached, as judged from spectra recorded for 5 h (data not shown). The most intense and strong positive band was located at 1623 cm^{-1}, which corresponds to amide-I $\nu_{(C=O)}$ carbonyl stretching. This band is characteristic of the presence of antiparallel β-sheets, which is also the case of the small amide-I′ band at 1695 cm^{-1} (40,41). The lower intensity band at 1526 cm^{-1} was assigned to the NH and CN bending (amide II) of the protein, which is characteristic of antiparallel β-sheet structures (40). A band at 1645 cm^{-1} also indicates the presence of some random coil structures. The amide I to amide I′ ratio was found to be ~8, suggesting that part of the protein forms an antiparallel β-sheet laying parallel to the interface plane. Indeed, when the PM-IRRAS spectrum of a protein present at the A/W interface displays a strong positive amide I band and a weak positive amide I′ band, associated with an amide I to amide I′ ratio of ~9, the antiparallel β-sheet is flat and parallel to the interface plane (34).

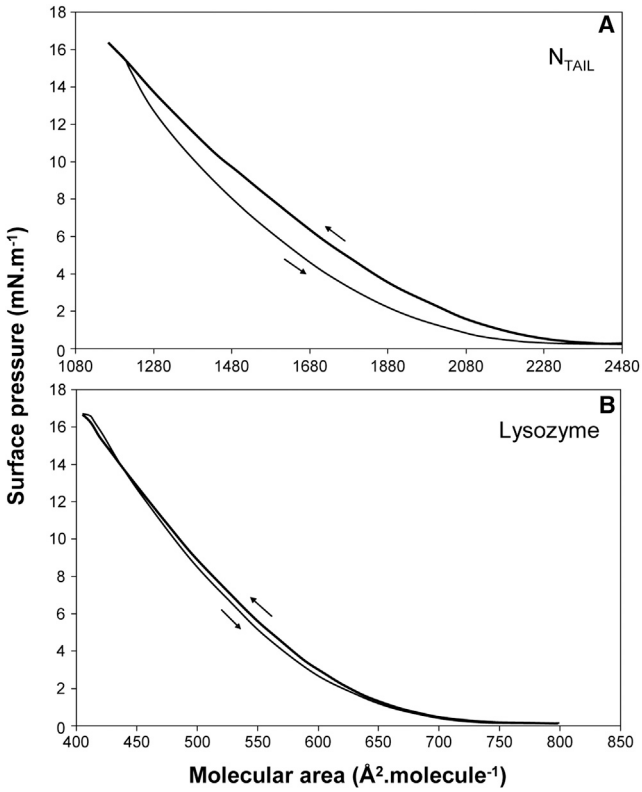


FIGURE 2 Compression/decompression of N_{TAIL} (*A*) and lysozyme (*B*) protein films formed at the air/water interface. For both proteins, the compression/decompression cycle was performed at a constant rate of 5 mm min^{-1}. Thick and thin lines correspond to compression and decompression, respectively, as also indicated by arrows. The subphase consists in 10 mM Tris/HCl buffer, pH 7.0, containing 100 mM NaCl, 21 mM $CaCl_2$, and 1 mM EDTA. Experiments were carried out in triplicate in a rectangular Teflon trough as described in the Materials and Methods. Only one representative experiment is shown here for both proteins.

PM-IRRAS spectra were also recorded after adsorption of N_{TAIL} onto an eggPC monolayer initially formed at a surface pressure of 4 mN m^{-1} and after the equilibrium surface pressure of ~15 mN m^{-1} was reached (see Adsorption of N_{TAIL}, Lysozyme, and eggPC at the A/W Interface and Interfacial Dilational Rheometry) for a more detailed study of N_{TAIL} interaction with eggPC monolayers). The spectrum of pure eggPC was subtracted from the composite spectrum obtained with the mixed monolayer, which allowed us to distinguish the characteristic contribution of N_{TAIL} to the signal (Fig. 3). The global intensity of the spectrum of N_{TAIL} adsorbed onto an eggPC monolayer was lower than the intensity recorded in the absence of phospholipids at the A/W interface, which can be due to lower amounts of protein present at the interface or to a lower detection of the protein in the presence of the lipid film. In any case, the resulting differential spectrum featured one main band at 1624 cm^{-1} and was assigned to the amide I vibration, which

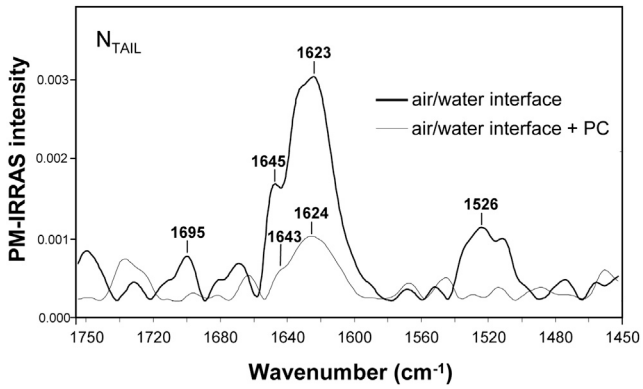


FIGURE 3 PM-IRRAS spectra of N_{TAIL} adsorbed at the air/water interface (*thick black line*) and on an eggPC monomolecular film formed at the air/water interface (*thin gray line*). The initial bulk concentration of N_{TAIL} was 0.5 μg mL^{-1} (or 32.7 nM). Data were collected at the equilibrium surface pressure (Π_e) after protein adsorption.

also indicates an antiparallel β-sheet folding of N_{TAIL} in the presence of phospholipids. The shoulder observed at 1643 cm^{-1} suggests that N_{TAIL} still has some random coil structure when adsorbed onto the lipid monolayer. The amide I′ and II bands were not observed in the presence of phospholipids, and N_{TAIL} orientation could not be estimated under these conditions.

Adsorption of N_{TAIL}, lysozyme, and eggPC at the A/W interface and interfacial dilational rheometry

We studied the adsorption of N_{TAIL}, lysozyme, and eggPC at the surface of air bubbles by measuring changes in surface pressure after injection of the protein (80 nM) or phospholipids (0.05% w/v final concentration) in the bulk phase (Fig. 4 *A*). Phospholipids were injected in the form of LUVs. The increase in the surface pressure was faster with eggPC than with N_{TAIL} and lysozyme, which both featured a lag phase of ~15 min before the surface pressure increase has reached its maximum rate. Subsequently, N_{TAIL} then displayed a faster adsorption kinetics compared to lysozyme. The surface pressures that were reached at equilibrium were 14.1 ± 0.3 mN m^{-1} for eggPC, 17.5 ± 0.9 mN m^{-1} for N_{TAIL}, and 17.1 ± 0.3 mN m^{-1} for lysozyme. The value obtained with lysozyme is identical to the surface pressure previously recorded with native lysozyme by Desfougères et al. (42), although the protein bulk concentration used in that previous study (0.1 mg mL^{-1} or 7 μM) was 87 times higher than the concentration we used here. The value obtained with eggPC is similar to the equilibrium surface pressure previously recorded by Mitsche et al. (43) using the same drop tensiometer.

Protein adsorptions in the presence of eggPC were also tested, but additional changes in surface pressure induced by the protein were weak and hardly interpretable (data not shown), probably because the surface pressure reached

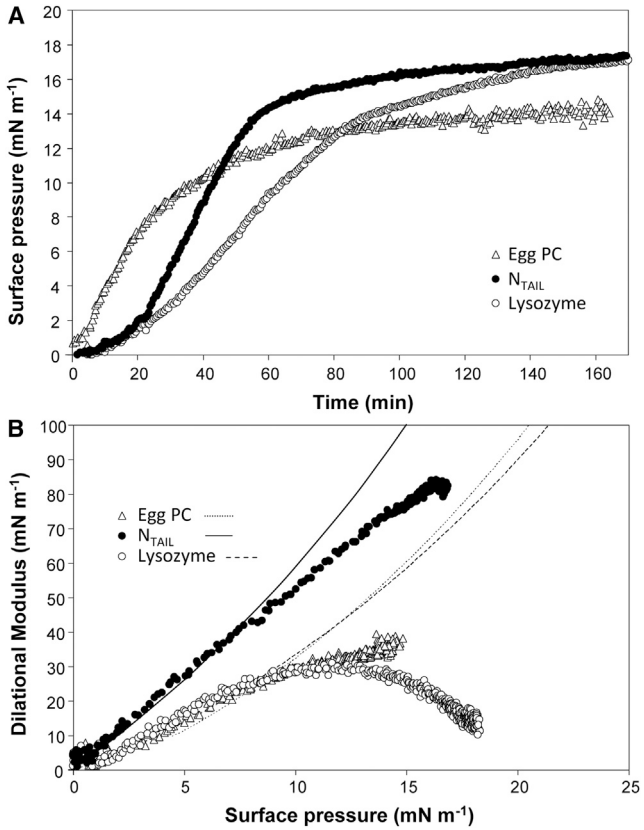


FIGURE 4 Characterization of N_{TAIL}, lysozyme, and eggPC at the air/water interface using the dynamic drop tensiometer. (*A*) Shown here is surface pressure as a function of time, and (*B*) dilational modulus as a function of surface pressure. The line in (*B*) represents theoretical models based on the Frumkin equation.

after eggPC injection was close to the critical surface pressure of penetration of both proteins. Dilational rheometry further confirmed that the interfacial properties were mainly controlled by phospholipids under these conditions (data not shown).

The mechanical response to compression/dilation of the protein and eggPC layers at the A/W interface was measured simultaneously to adsorption by using sinusoidal oscillations of the air-bubble volume and thus of interfacial area A ($\Delta A/A = 0.25$ at a frequency of 0.2 Hz). The surface dilational modulus E (Fig. 4 *B*) and its elastic (E') and viscous (E'') components (Fig. S2) were continuously determined for both proteins and eggPC, and were plotted as a function of surface pressure Π.

The dilational modulus recorded for lysozyme as a function of the surface pressure showed a bell-shaped variation with a maximum value of 30 mN m^{-1} at a surface pressure of ~12 mN m^{-1}. Before the inflection, the dilational modulus of lysozyme was similar to that of phospholipids (Fig. 4 *B*). The lysozyme layer at the A/W interface showed a quasi-pure elastic behavior as indicated by the E''/E' ratio (or tangent of the ϕ-viscous phase angle), which was 0.071 at 15 mN m^{-1} (Fig. S2). The ϕ-viscous phase angle was

therefore close to zero, which indicates no shift between surface area of the bubble and surface tension variations when the frequency of sinusoidal oscillations was 0.2 Hz. We also performed dilational rheometry experiments at various frequencies from 0.1 to 1 Hz, and always observed a very low phase angle for lysozyme (data not shown). The dilational modulus observed with N_{TAIL} was much higher, reaching values of ~80 mN m^{-1}, and it showed a linear increase with surface pressure up to 15 mN m^{-1} (Fig. 4 *B*). This indicates that N_{TAIL} molecules have a much stronger interaction between each other compared to lysozyme and eggPC molecules. Compared to lysozyme, the N_{TAIL} layer at the A/W interface also showed a viscoelastic behavior with a significant viscous modulus and an E''/E' ratio of 0.12 at 15 mN m^{-1}.

The E (Π) data points were then fitted with a 2D solution treatment (see Eqs. 6 and 7 in Materials and Methods) to provide a description of $E(\Pi)$ variations in the elastic range where E is dominated by the equation of state, i.e., for values of $\Pi < 10$ mN m^{-1} (38). A good fit was obtained for surface pressures below 8 mN m^{-1} for N_{TAIL}, lysozyme, and eggPC (Fig. 4 *B*; Table 2), with molecular areas close to those estimated from N_{TAIL} and lysozyme compression isotherms (Fig. 2) and previous experiments with eggPC (90 $Å^2$ $molecule^{-1}$ (43)). Above this surface pressure, deviations occur that probably reflect molecular rearrangements of the surfactants at the A/W interface. This treatment allowed estimating the interaction parameter H corresponding to the molar enthalpy of mixing at the surface, and the size factor S that corresponds to the solvent molecule equivalents displaced by the surfactant (protein or eggPC) upon adsorption at the A/W interface. Negative values for H represent attractive forces between surfactants and solvent (water) and repulsive forces between surfactants at interfaces, whereas positive values indicate attractive interactions between the surfactant molecules at the interface (37). We observed this situation in all cases, but these interactions were stronger for N_{TAIL} ($H = 0.65$ RT) than for lysozyme ($H = 0.2$ RT), whereas an intermediate value was obtained for eggPC (Table 2). Based on S values, N_{TAIL} ($S = 120$) displaces more solvent molecules from the interface than lysozyme ($S = 37$) and eggPC ($S = 5.5$).

TABLE 2 Parameter Values Used for Fitting Experimental Data of Dilational Modulus Variations versus Surface Pressure with the 2D Solution Model

Surfactant/Solute	Molecular Area ω_1 ($Å^2$ per Molecule)	*H/RT*	*S*
EggPC	90	0.5	5.5
Lysozyme	600	0.2	37
N_{TAIL}	2000	0.65	120

For each surfactant or solute, the molecular area used for calculations was the area occupied by the surfactant or solute at the maximum or saturation adsorption. It was estimated from monolayer compression isotherms for N_{TAIL} and lysozyme (Fig. 2) or from a previous study for eggPC (43). Dilational modulus, E; surface pressure, Π.

The initial variation of the dilational modulus with surface pressure ($\Delta E/\Delta\Pi$) was also found to be higher with N_{TAIL} (5.46) than with lysozyme (2.84) and eggPC (2.64), which supports stronger interactions between N_{TAIL} molecules at the interface.

Adsorption of N_{TAIL} and lysozyme onto phospholipid monomolecular films

Protein adsorption onto eggPC films formed at the A/W interface was monitored by recording the increase in surface pressure Π as a function of time after protein injection in the bulk phase below the phospholipid film. Fig. 5 shows typical adsorption kinetics recorded with N_{TAIL} and lysozyme using a bulk concentration of 60 nM for each protein and an initial surface pressure of 4 mN m^{-1}. N_{TAIL} adsorption/penetration onto the phospholipid film was found to induce a larger increase in surface pressure ($\Delta\Pi$) than lysozyme. The maximum increase in surface pressure $\Delta\Pi_{max}$ was studied as a function of the initial surface pressure Π_i of the eggPC monolayers before protein injection (Fig. 6). The $\Delta\Pi_{max}(\Pi_i)$ plots show a linear decrease of $\Delta\Pi_{max}$ with increasing Π_i and a linear regression fit allowed the estimation of the critical surface pressure of penetration (Π_c) above which no increase in surface pressure occurs ($\Delta\Pi_{max} = 0$) (44). Π_c was found to be 18.2 ± 0.2 and 11.9 ± 0.1 mN m^{-1} for N_{TAIL} and lysozyme, respectively, indicating a better capacity of N_{TAIL} for binding to a phospholipid monolayer compared to lysozyme. $\Delta\Pi_0$ (y intercept of the curve corresponding to $\Pi_i = 0$) was

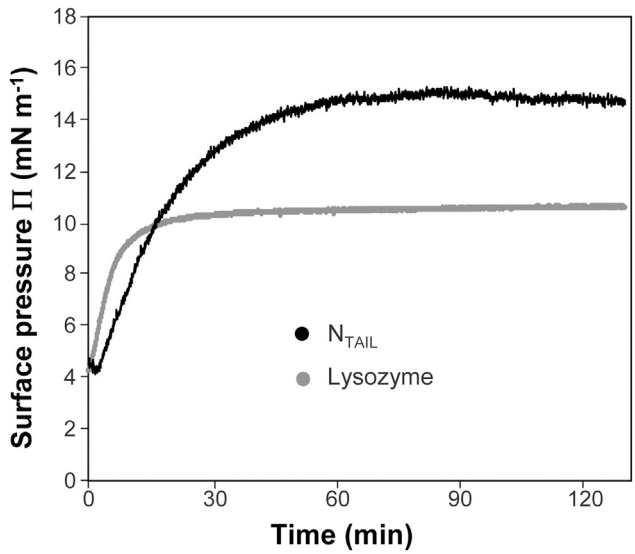


FIGURE 5 Typical recordings (surface pressure as a function of time) of N_{TAIL} and lysozyme adsorption onto a phosphatidylcholine monolayer spread at the air/water interface. The proteins (60 nM final concentration) were injected into the aqueous phase (10 mM Tris/HCl buffer, pH 7.0, containing 100 mM NaCl, 21 mM $CaCl_2$, and 1 mM EDTA) and the surface pressure increase was continuously recorded as described in Materials and Methods. The initial surface pressure of the phosphatidylcholine monolayer was 4 mN m^{-1}.

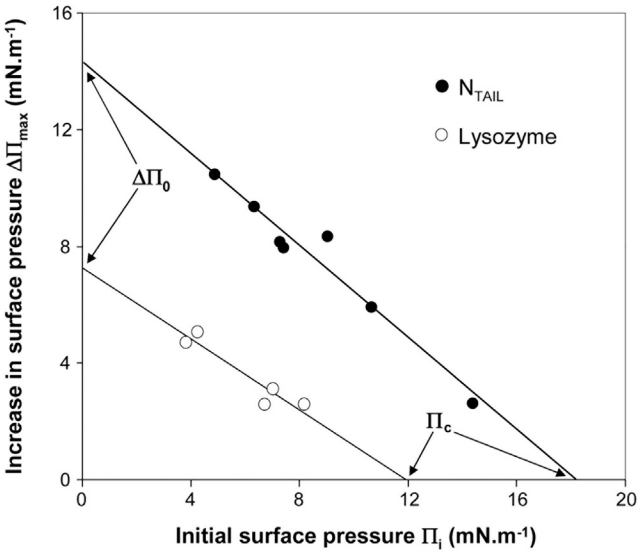


FIGURE 6 Variations in surface pressure upon adsorption of NTAIL and lysozyme onto eggPC monomolecular films. Proteins (40 nM final concentration) were injected into the aqueous phase (10 mM Tris/HCl buffer, pH 7.0, 100 mM NaCl, 21 mM $CaCl_2$, and 1 mM EDTA) below the lipid film at various initial surface pressures (Π_i) ranging from 4 to 14 mN m^{-1}. The maximum increase in surface pressure ($\Delta\Pi_{max}$) was then recorded and plotted as a function of Π_i. The critical surface pressure for penetration (Π_c; intercept of the linear regression with the *x* axis) and $\Delta\Pi_0$ (intercept of the linear regression with the *y* axis) were determined. Experiments were carried out in a cylindrical Teflon trough, as described in the Materials and Methods.

also deduced from the same plot (Fig. 6). In both cases, the $\Delta\Pi_0$ values (14.3 mN m^{-1} for N_{TAIL} and 7.3 mN m^{-1} for lysozyme) were lower than the corresponding Π_c values, which is consistent with an insertion surface pressure and favorable interactions between the protein and the phospholipid film (45). The critical surface pressure of penetration estimated for lysozyme is close to the value (10 mN m^{-1}) reported in a previous study (46).

Taking into account the Π_c values, the kinetic parameters of N_{TAIL} and lysozyme adsorption onto eggPC monolayers were determined at a surface pressure of $\Pi_i = 4$ mN m^{-1}. A series of adsorption kinetics were performed by varying protein concentrations in the range of 20–80 nM. Adsorption (k_a) and desorption (k_d) rate constants were determined by fitting the experimental data points to the Langmuir adsorption equation (Eq. 1). The linear regression of σ as a function of protein concentration (Fig. S3) gave direct access to k_a and k_d constants and then to the adsorption equilibrium constant, K_{Ads} and dissociation constant, K_D (Table 3). At $\Pi_i = 4$ mN m^{-1}, the equilibrium surface pressure ($\Pi_e = 14.6 \pm 1.3$ mN m^{-1}) and K_{Ads} ($3.3 \pm 0.2 \times 10^8$ M^{-1}) estimated for N_{TAIL} were nearly twice the values determined for lysozyme ($\Pi_e = 8.8 \pm 1.9$ mN m^{-1} and $K_{Ads} = 1.5 \pm 0.1 \times 10^8$ M^{-1}).

The determination of K_D further allowed us to estimate the interfacial concentration (Γ_E*, molecule cm^{-2}) and the molar fraction (Φ_E*$_{(\%)}$, mol %) of the protein adsorbed onto eggPC films at the equilibrium surface pressure, using Eqs. 2 and 3, respectively. As expected, Γ_E* and Φ_E*$_{(\%)}$ values for N_{TAIL} were almost twice those determined for lysozyme (Table 4). The surface area occupied by one molecule of the adsorbed protein (A_E*) was further calculated using Eq. 4 and was found to be $972 \geq 89$ Å^2 molecule^{-1} for N_{TAIL} and 1513 ± 76 Å^2 molecule^{-1} for lysozyme, respectively.

Using the same methodological approach, we assessed the binding parameters at $\Pi_i = 10$ mN m^{-1}. As expected, no variation in surface pressure was recorded for lysozyme, thus preventing the determination of adsorption parameters for this protein. With N_{TAIL}, K_{Ads} as well as Γ_E* and Φ_E*$_{(\%)}$ values were in the same order of magnitude as those obtained at $\Pi_i = 4$ mN m^{-1}, suggesting comparable adsorption properties of the protein at the two tested Π_i values (Table 4). However, the A_E* value of 638 ± 47 Å^2 molecule^{-1} estimated for N_{TAIL} at 10 mN m^{-1} was 1.5-fold lower than the apparent molecular area estimated at 4 mN m^{-1}, indicating that either N_{TAIL} penetration into the phospholipid layer decreased or that protein conformation was more compact when the surface pressure increased.

DISCUSSION

Comparison of N_{TAIL} and lysozyme structures upon adsorption at the A/W interface

Once spread at the A/W interface, N_{TAIL} shows a molecular area of 1868 ± 100 Å^2, a value that is much higher than the molecular area of lysozyme (616 ± 15 Å^2) although these proteins have a similar molecular mass. The estimated molecular area of N_{TAIL} fits well with the maximum section of 2124 ± 327 Å^2 estimated from the hydrodynamic radius (R_H) of 26 ± 2 Å, as experimentally determined for N_{TAIL} using gel-filtration chromatography (23). Such a large

TABLE 3 Kinetics Constants Derived from the Adsorption Kinetics of N_{TAIL} and Lysozyme onto EggPC Films at pH 7.0 and at Two Initial Surface Pressures

Protein	Π_i (mN m^{-1})	k_a (M^{-1} s^{-1})	k_d (s^{-1})	K_{Ads} (M^{-1})	K_D (nM)
Lysozyme	4	$1.9 (\pm 0.1) \times 10^4$	$1.3 (\pm 0.0003) \times 10^{-4}$	$1.5 (\pm 0.1) \times 10^8$	6.67
N_{TAIL}	4	$1.3 (\pm 0.001) \times 10^4$	$0.4 (\pm 0.1) \times 10^{-4}$	$3.3 (\pm 0.2) \times 10^8$	3.45
	10	$2.0 (\pm 0.1) \times 10^4$	$0.9 (\pm 0.02) \times 10^{-4}$	$2.9 (\pm 0.2) \times 10^8$	3.03

Values of the adsorption (k_a) and desorption (k_d) constants were determined from the slope and *y* intercept, respectively, of the linear plot of σ versus protein concentration (Eq. 1; Fig. S3). $K_{Ads} = k_a/k_d$ and $K_D = 1/K_{Ads}$. Values are mean $\pm$ SD ($n = 3$).

TABLE 4 Characteristic Values of N_{TAIL} and Lysozyme Adsorption onto EggPC films at pH 7.0 and at Two Initial Surface Pressures

Protein	Π_i (mN m^{-1})	Π_e (mN m^{-1})	Γ_E* (Molecule cm^{-2})	Φ_E*$_{(\%)}$ (Mol %)	A_E* (Å^2 Molecule^{-1})
Lysozyme	4	8.8 ± 1.9	5.4×10^{12}	12.8 ± 5.0	1513 ± 76
N_{TAIL}	4	14.6 ± 1.3	10.6×10^{12}	25.0 ± 9.2	972 ± 89
	10	17.6 ± 1.1	9.6×10^{12}	22.8 ± 7.3	638 ± 47

Π_i, initial surface pressure; Π_e, surface pressure at equilibrium; Γ_E*, protein interfacial concentration; Φ_E*$_{(\%)}$, molar fraction of the protein adsorbed onto eggPC films; A_E*, molecular area occupied by the protein adsorbed onto eggPC films; Γ_E*, Φ_E*$_{(\%)}$, and A_E* values were estimated by indirect calculation using Eqs. 2, 3 and 4 for an initial protein concentration in the subphase (C_{E0}) of 60 nM. Values are mean ± SD ($n = 3$).

molecular area suggests that N_{TAIL} polypeptide is fully spread over the A/W interface, which fits with the PM-IRRAS spectrum of N_{TAIL} showing characteristic bands of antiparallel β-strands lying parallel to the interface plane (Fig. 3). So far, only a local α-helical folding taking place in a short α-helical molecular recognition element (amino acids 486–502) has been reported for N_{TAIL} upon interaction with its physiological partner, the X domain of the phosphoprotein (P_{XD}) (Fig. 7) (18,20,21,23). Here, we show that the intrinsically disordered N_{TAIL} domain can gain a distinct secondary structure upon adsorption at the A/W interface where it folds into a flat antiparallel β-sheet (Fig. 7). It is worth noticing that a partial folding of the homologous measles virus N_{TAIL} into an antiparallel β-sheet has been predicted by combining homology modeling and all-atom Monte Carlo-based simulations using NMR chemical shifts

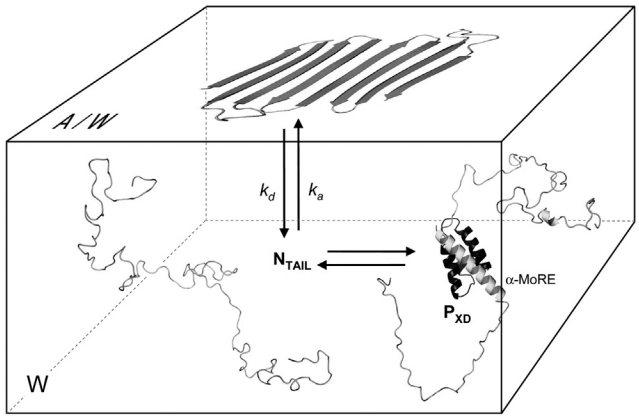


FIGURE 7 Schematic representation of N_{TAIL} folding upon adsorption at the A/W interface or interaction with its physiological partner P_{XD} (*black α-helical* bundle) in the water phase (W). Secondary structure elements are indicated in light gray (α-helices) and dark gray (β-strands) for NTAIL and black (α-helices) for PXD. A conformational ensemble of N_{TAIL} in solution was built using the Flexible-Meccano software program (62), and two conformers were selected to illustrate the complete random coil structure of N_{TAIL} alone in solution and the partly structured N_{TAIL} showing an α-helix (α-MoRE region) upon interaction with its physiological partner, the X domain of the viral phosphoprotein (P_{XD}). The 3D model of the N_{TAIL}-P_{XD} complex was built using the N_{TAIL} conformer with the α-MoRE region folded as an α-helix and the known 3D structure of HeV P_{XD} (PDB: 4HEO (21)) with the N_{TAIL} α-helix in a parallel conformation with respect to P_{XD} according to (63). The N_{TAIL} conformer adopting an antiparallel β-strand fold at the A/W interface is a free drawing. All structural models were drawn using the PyMOL Molecular Graphics System, Version 1.2r3pre (Schrödinger, New York, NY) (64).

as restraints. The surface-accessible solvent area of the resulting structural model was in nice agreement with the value experimentally determined using ESI-MS (47).

The folding of N_{TAIL} into an antiparallel β-sheet at the A/W interface is reminiscent of the structural rearrangement undergone by many proteins upon adsorption at the interface between water and a hydrophobic phase. For instance, the prion-forming domain of the fungal amyloid protein HET (48) and lysozyme (49) can adopt an antiparallel β-sheet at the A/W interface. Nevertheless, N_{TAIL} folding into a β-sheet appears as a fast process according to PM-IRRAS analysis. Studies with globular proteins suggest a much slower process to form β-structures and in some cases, no structural rearrangement at all (49). This is well illustrated by the numerous studies that have been dedicated to the structure of lysozyme upon adsorption at the A/W interface using various experimental approaches. It is often stated that lysozyme, like other globular proteins, is able to form strong interfacial protein films because of its ability to unfold upon adsorption. It was for instance observed by PM-IRRAS and FTIR spectroscopy that lysozyme adsorbed at the A/W interface displayed predominantly an antiparallel β-sheet structure (49,50). Other studies using neutron reflectivity and measurements of lysozyme layer thickness at the A/W interface have, however, concluded that lysozyme does not undergo significant unfolding at the interface (51–53). In a more recent study of native lysozyme at the A/W interface by AFM, ellipsometry, and PM-IRRAS, it was shown that this protein forms a smooth layer with an apparent film thickness of 3 nm (42). Time-lapse PM-IRRAS analysis of this film showed that lysozyme adsorbed at the A/W interface has a majority of α-helical content, as judged from the presence of amide I and amide II bands at 1657 and 1540 cm^{-1}, respectively (42). Those data therefore suggest that lysozyme adsorbed at the A/W interface preserves its structure, at least transiently. The 3D structure of lysozyme in solution is close to a prolate spheroid with a long axis of 46 Å and two short axes of 26 Å (estimated from PDB: 1LYZ). The protein section perpendicular to the long axis has a maximum area of ~530 Å^2, a value that is rather close to the molecular area we estimated here for lysozyme at the A/W interface (616 ± 15 Å^2; Fig. 2 *B*). One can therefore reasonably assume that lysozyme remains folded upon adsorption at the A/W interface with its long axis tending to be oriented perpendicularly to the interface plane upon

compression of the protein layer. The appearance and increase over time of additional bands characteristic of β-sheet formation (1682 and 1625 cm^{-1}) indicates, however, that lysozyme slowly tends to rearrange at the A/W interface (42). The lack of a general agreement as to the extent of unfolding that lysozyme undergoes at the A/W interface (51) may in fact result from differences in experimental conditions and time frames for the acquisition of spectra during a slow rearrangement process (54,55). IDPs like N_{TAIL} do not have to unfold before forming β-sheet structures at interfaces, and hence the energetic pathway seems more favorable to readily form these structures upon adsorption.

Characteristics of N_{TAIL} and lysozyme layers at the A/W interface

The lysozyme layer at the A/W interface shows a quasi-pure elastic behavior, as indicated by very low viscous phase angles (Fig. S2) and a minor hysteresis of Π(A) upon compression/decompression (Fig. 2). Because lysozyme seemingly does not unfold at the A/W interface in the time frame of our experiments, the behavior of the protein layer may result from changes in the orientation of lysozyme molecules upon compression. Indeed, lysozyme 3D structure has an ellipsoidal shape. Its large axis may be initially parallel to interface plane and then progressively tilted upon compression and tending to be perpendicular to the interface plane (Fig. 8 *A*).

Compared to lysozyme, N_{TAIL} layer at A/W interface shows a higher dilational modulus (Fig. 4 *B*). The formation of a highly viscoelastic film, strong intermolecular interactions, and significant viscosity (Fig. S2) probably results from the fact that the N_{TAIL} polypeptide is totally spread at the air-water interface and structured in an antiparallel β-sheet (Fig. 3). The large hysteresis observed upon compression/decompression of N_{TAIL} film may result from the overlap of β-sheets upon compression of the protein layer and intermolecular interactions delaying the spreading of all N_{TAIL} molecules upon decompression (Fig. 8 *B*).

N_{TAIL} and lysozyme interactions with phospholipid monomolecular films

As observed at the A/W interface, N_{TAIL} presents a better adsorption capacity onto an eggPC monolayer compared to lysozyme (Figs. 5 and 6; Table 3). The molecular area of N_{TAIL} adsorbed onto the eggPC monolayer at an initial surface pressure of 4 mN m^{-1} (972 $\pm$ 89 $Å^2$) is, however, twofold lower than the molecular area estimated for the protein alone at the A/W interface. N_{TAIL} is therefore not totally spread at the interface in the presence of phospholipids, and part of the molecule may remain in the water phase. N_{TAIL} exclusion from the interface increases with the compression of the phospholipid monolayer (molecular area of 638 $\pm$ 47 $Å^2$ at an initial surface pressure 10 mN m^{-1}) until a critical surface pressure of penetration is reached (18.2 $\pm$ 0.2 mN m^{-1}; Fig. 6). PM-IRRAS analysis reveals that the fraction of N_{TAIL} bound to the phospholipid monolayer folds in an antiparallel β-sheet, as observed with the protein spread at the A/W interface (Fig. 3).

A reverse situation is observed with lysozyme that shows a 2.4-fold increase in molecular area (1513 $\pm$ 76 $Å^2$) when a phospholipid monolayer is present at the A/W interface. Because lysozyme has an ellipsoidal shape, this may indicate that the lysozyme molecules have their large axis parallel to interface plane in the presence of phospholipids,

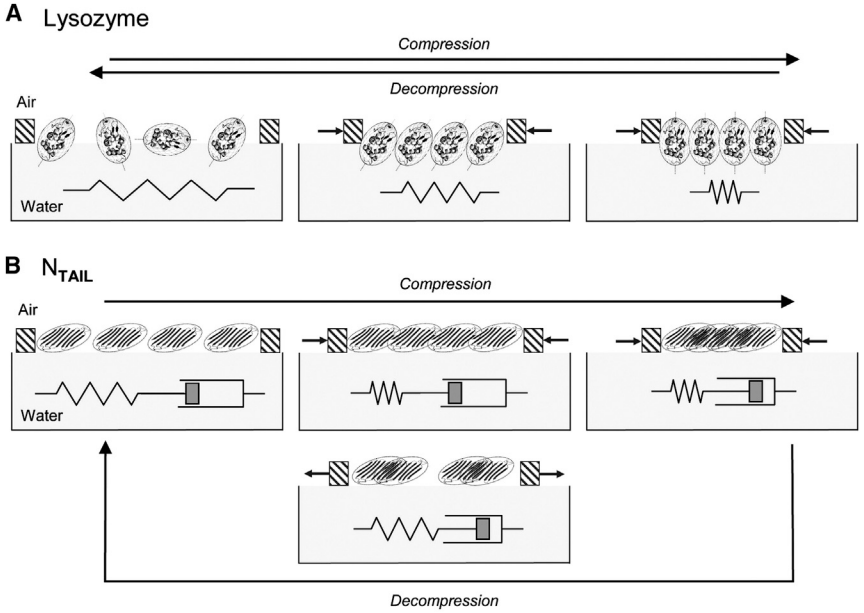


FIGURE 8 Schematic representation of lysozyme and N_{TAIL} behavior at the A/W interface upon compression/decompression of the protein layer. The shape and orientation of the lysozyme molecule (*A*) is based on previous data on its structure in solution (PDB: 1LYZ) and at the air-water interface (PM-IRRAS (42)), as well as on the molecular area estimated in this work (Fig. 2 *B*). Lysozyme is represented as a prolate spheroid with a long axis of 46 Å and two small axes of 26 Å, with various orientations depending on the surface pressure. The N_{TAIL} molecules at the A/W interface (*B*) are shown as a single ellipsoid antiparallel β-sheet having a large axis of 120 Å (maximum dimension determined by SAXS in the case of the homologous N_{TAIL} protein from the cognate measles virus (65)) and an area of ~2000 $Å^2$ as determined in this work (Fig. 2 *A*). The viscoelastic behavior of the protein layers at the A/W interface is schematized by a spring only for lysozyme (purely elastic) and a spring combined with a damper (Maxwell model) for N_{TAIL} to illustrate the viscous component of N_{TAIL} behavior.

whereas the large axis of lysozyme tends to be perpendicular to the interface plane in the absence of phospholipids. More probably, lysozyme may unfold upon adsorption onto phospholipid monolayers, which would result in a molecular area larger than the maximum section estimated from lysozyme 3D structure. Lysozyme unfolding and aggregation has been previously observed upon membrane association and interactions with phospholipids (56).

Comparison of N_{TAIL} and other IDPs undergoing disorder-to-order transitions at interfaces

This study provides the evidence that the intrinsically disordered N_{TAIL} undergoes a disorder-to-order transition at the A/W interface and adopts secondary structure elements (antiparallel β-strands) that are distinct from those observed in solution (α-helix) upon interaction with its physiological partner P_{XD} (Fig. 7). Presently, this β-transition cannot be associated with any biological mechanism. Indeed, N_{TAIL} is part of the Hendra virus nucleoprotein involved in the viral replication machinery and genome encapsidation (18). There is no evidence of any N_{TAIL} interaction with membranes or other biological interfaces. Nevertheless, its characterization at the A/W interface extends our knowledge on the interfacial behavior of IDPs. All IDPs studied so far present significant surface activity and undergo disorder-to-order transitions at the A/W and membrane interfaces. They can either adopt an α-helical conformation like α-synuclein (14,15) and amyloid β-peptide (Aβ) (5) or a β-sheet conformation like the prion-forming domain of the fungal amyloid protein HET (48), the human Prion amyloidogenic determinant (57), and N_{TAIL}. The tau protein also adopts a more compact conformation with a density similar to that of a folded protein upon adsorption at the A/W interface, and this may render it aggregation-competent (6). In all cases, the hydrophobic side of the interface seems to facilitate conformational changes further leading to protein aggregation.

Proteins possessing both structured and unstructured regions may, however, behave differently. A typical example is given by the characterization of ZipA, a protein involved in the cell division machinery of *Escherichia coli*. It is a multidomain membrane-bound protein of 328 amino acids, which contains two terminal folded domains connected by an unfolded segment of ~150 amino acids (58). Whereas the α-helical transmembrane domain at the N terminus anchors the protein to the cytoplasmic membrane, the globular C-terminal domain is responsible for the interaction of ZipA with a protein partner, FtsZ, involved in bacterial division. A study of ZipA at the A/W interface suggests that the protein undergoes a coil-to-brush conformational transition at high surface pressure, but preserves the disordered nature of its linker (58).

The ability of N_{TAIL} to adopt a completely different fold at the A/W interface may reflect the inherent plasticity that typifies IDPs and the lack of a robust folding nucleus as typically observed in globular proteins. The interface thus sculpts the IDP in a manner that is reminiscent of the partner-templated folding proposed for the intrinsically disordered transactivation domain of the c-Myb transcription factor (59). It is therefore tempting to speculate that this templated folding can be a general mechanism of IDPs that may enable them to achieve specific binding to multiple, structurally different partners, as already proposed (59).

CONCLUSIONS

The intrinsically disordered protein N_{TAIL} presents a significant surface activity and adsorbs rapidly at the A/W interface to form a highly viscoelastic film. This interfacial behavior probably results from the fact that N_{TAIL} rapidly folds into an antiparallel β-sheet structure and presents strong intermolecular interactions. N_{TAIL} folding at the A/W interface appears to be a much faster process than lysozyme rearrangement, probably due to the lower energy barrier required for an IDP to fold into antiparallel β-sheet while the globular 3D structure of lysozyme has first to be disrupted. As a consequence, lysozyme mainly keeps its tertiary structure at the A/W interface in the timeframe of our experiments, and the protein film shows a purely elastic behavior.

Apart from fundamental considerations, the properties of IDPs at interfaces may be useful for engineering protein layers at various interfaces (i.e., stabilization of emulsions, blocking the adsorption of other proteins/enzymes (60)). Folding at interfaces of disordered peptides has also been used to specifically turn on the lytic activity of anticancer cationic peptides at the electronegative surface of cancer cells. These peptides were designed to remain unfolded and inactive in aqueous solution, but they preferentially adopt an amphiphilic β-hairpin structure capable of membrane disruption upon interaction with cancer cell membrane (61). The association of IDPs with interfaces and/or membranes may therefore lead to various applications.

SUPPORTING MATERIAL

Three figures are available at http://www.biophysj.org/biophysj/supplemental/S0006-3495(17)31123-2.

AUTHOR CONTRIBUTIONS

A.B. was involved in the conception and design of the study; in acquisition, analysis, and interpretation of data from monolayer and interfacial rheology experiments; and in drafting the article. J.H. was involved in the acquisition, analysis, and interpretation of data related to the production of proteins. A.C. was involved in the conception and design of the study, in the development of the oil drop tensiometer for interfacial rheology experiments, and analysis of tensiometry data. O.M. was involved in the acquisition, analysis, and interpretation of data from PM-IRRAS experiments. A.G.-E. was involved in the analysis and interpretation of data from PM-IRRAS

experiments, and in drafting and revising the article for important intellectual content. J.-F.C. was involved in the analysis and interpretation of data from monolayer experiments. S.L. was involved in the conception and design of the study, in drafting the article, and revising it critically for important intellectual content. F.C. was involved in the conception and design of the study, in drafting the article, revising it critically for important intellectual content, and in final approval of the version to be submitted. All authors were involved in the final approval of the version to be submitted.

ACKNOWLEDGMENTS

We are grateful to Marion Dosnon (AFMB Laboratory, Marseille) for her assistance during the production and purification of N_{TAIL}, to Vanessa Point (EIPL Laboratory, Marseille) for preliminary monolayer experiments with lysozyme, and to Eliora Maruani (EIPL Laboratory, Marseille) for performing some experiments with the drop tensiometer.

This work was supported by the Centre National de la Recherche Scientifique (CNRS).

REFERENCES

1. Dunker, A. K., M. M. Babu, …, V. N. Uversky. 2013. What's in a name? Why these proteins are intrinsically disordered. *Intrinsically Disord. Proteins.* 1:e24157.
2. Fink, A. L. 2006. The aggregation and fibrillation of α-synuclein. *Acc. Chem. Res.* 39:628–634.
3. Galvagnion, C., J. W. Brown, …, C. M. Dobson. 2016. Chemical properties of lipids strongly affect the kinetics of the membrane-induced aggregation of α-synuclein. *Proc. Natl. Acad. Sci. USA.* 113:7065–7070.
4. Galvagnion, C., A. K. Buell, …, C. M. Dobson. 2015. Lipid vesicles trigger α-synuclein aggregation by stimulating primary nucleation. *Nat. Chem. Biol.* 11:229–234.
5. Jiang, D., K. L. Dinh, …, F. Zhou. 2009. A kinetic model for β-amyloid adsorption at the air/solution interface and its implication to the beta-amyloid aggregation process. *J. Phys. Chem. B.* 113:3160–3168.
6. Jones, E. M., M. Dubey, …, E. Y. Chi. 2012. Interaction of tau protein with model lipid membranes induces tau structural compaction and membrane disruption. *Biochemistry.* 51:2539–2550.
7. Wright, P. E., and H. J. Dyson. 1999. Intrinsically unstructured proteins: re-assessing the protein structure-function paradigm. *J. Mol. Biol.* 293:321–331.
8. Dunker, A. K., J. D. Lawson, …, Z. Obradovic. 2001. Intrinsically disordered protein. *J. Mol. Graph. Model.* 19:26–59.
9. Uversky, V. N. 2002. Natively unfolded proteins: a point where biology waits for physics. *Protein Sci.* 11:739–756.
10. Habchi, J., P. Tompa, …, V. N. Uversky. 2014. Introducing protein intrinsic disorder. *Chem. Rev.* 114:6561–6588.
11. Longhi, S., P. Lieutaud, and B. Canard. 2010. Conformational disorder. *Methods Mol. Biol.* 609:307–325.
12. Lieutaud, P., F. Ferron, …, S. Longhi. 2013. Predicting protein disorder and induced folding: a practical approach. *In* Advances in Protein and Peptide Sciences. B. Dunn, ed. Bentham Science Publishers, Emirate of Sharjah, United Arab Emirates, pp. 441–492.
13. Bokor, M., V. Csizmók, …, K. Tompa. 2005. NMR relaxation studies on the hydrate layer of intrinsically unstructured proteins. *Biophys. J.* 88:2030–2037.
14. Wang, C., N. Shah, …, R. M. Leblanc. 2010. α-synuclein in α-helical conformation at air-water interface: implication of conformation and orientation changes during its accumulation/aggregation. *Chem. Commun. (Camb.).* 46:6702–6704.
15. Davidson, W. S., A. Jonas, …, J. M. George. 1998. Stabilization of α-synuclein secondary structure upon binding to synthetic membranes. *J. Biol. Chem.* 273:9443–9449.
16. Fusco, G., A. De Simone, …, G. Veglia. 2014. Direct observation of the three regions in α-synuclein that determine its membrane-bound behaviour. *Nat. Commun.* 5:3827.
17. Fusco, G., A. De Simone, …, C. M. Dobson. 2016. Structural ensembles of membrane-bound α-synuclein reveal the molecular determinants of synaptic vesicle affinity. *Sci. Rep.* 6:27125.
18. Habchi, J., and S. Longhi. 2012. Structural disorder within paramyxovirus nucleoproteins and phosphoproteins. *Mol. Biosyst.* 8:69–81.
19. Longhi, S., L. M. Bloyet, …, D. Gerlier. 2017. How order and disorder within paramyxoviral nucleoproteins and phosphoproteins orchestrate the molecular interplay of transcription and replication. *Cell. Mol. Life Sci.* 74:3091–3118.
20. Habchi, J., L. Mamelli, …, S. Longhi. 2010. Structural disorder within Henipavirus nucleoprotein and phosphoprotein: from predictions to experimental assessment. *PLoS One.* 5:e11684.
21. Communie, G., J. Habchi, …, M. Blackledge. 2013. Atomic resolution description of the interaction between the nucleoprotein and phosphoprotein of Hendra virus. *PLoS Pathog.* 9:e1003631.
22. Martinho, M., J. Habchi, …, S. Longhi. 2013. Assessing induced folding within the intrinsically disordered C-terminal domain of the Henipavirus nucleoproteins by site-directed spin labeling EPR spectroscopy. *J. Biomol. Struct. Dyn.* 31:453–471.
23. Habchi, J., S. Blangy, …, S. Longhi. 2011. Characterization of the interactions between the nucleoprotein and the phosphoprotein of Henipavirus. *J. Biol. Chem.* 286:13583–13602.
24. Callebaut, I., G. Labesse, …, J. P. Mornon. 1997. Deciphering protein sequence information through hydrophobic cluster analysis (HCA): current status and perspectives. *Cell. Mol. Life Sci.* 53:621–645.
25. Whitmore, L., and B. A. Wallace. 2004. DICHROWEB, an online server for protein secondary structure analyses from circular dichroism spectroscopic data. *Nucleic Acids Res.* 32:W668–W673.
26. Whitmore, L., and B. A. Wallace. 2008. Protein secondary structure analyses from circular dichroism spectroscopy: methods and reference databases. *Biopolymers.* 89:392–400.
27. Verger, R., and G. H. De Haas. 1973. Enzyme reactions in a membrane model. 1. A new technique to study enzyme reactions in monolayers. *Chem. Phys. Lipids.* 10:127–136.
28. Bénarouche, A., V. Point, …, J. F. Cavalier. 2013. New insights into the pH-dependent interfacial adsorption of dog gastric lipase using the monolayer technique. *Colloids Surf. B Biointerfaces.* 111:306–312.
29. Pieroni, G., and R. Verger. 1979. Hydrolysis of mixed monomolecular films of triglyceride/lecithin by pancreatic lipase. *J. Biol. Chem.* 254:10090–10094.
30. Bénarouche, A., L. Sams, …, F. Carrière. 2017. Studying gastric lipase adsorption onto phospholipid monolayers by surface tensiometry, ellipsometry, and atomic force microscopy. *Methods Enzymol.* 583: 255–278.
31. Panaiotov, I., and R. Verger. 2000. Enzymatic reactions at interfaces: interfacial and temporal organization of enzymatic lipolysis. *In* Physical Chemistry of Biological Interfaces. A. Baszkin and W. Norde, eds. Marcel Dekker, New York, Basel, pp. 359–400.
32. Blaudez, D., J.-M. Turlet, …, B. Desbat. 1996. Investigations at the air/water interface using polarization modulation IR spectroscopy. *J. Chem. Soc., Faraday Trans.* 92:525–530.
33. Blaudez, D., T. Buffeteau, …, J. M. Turlet. 1994. Polarization modulation FTIR spectroscopy at the air-water interface. *Thin Solid Films.* 242:146–150.
34. Castano, S., B. Desbat, and J. Dufourcq. 2000. Ideally amphipathic β-sheeted peptides at interfaces: structure, orientation, affinities for lipids and hemolytic activity of KL_mK peptides. *Biochim. Biophys. Acta.* 1463:65–80.
35. Castano, S., B. Desbat, …, J. Dufourcq. 1999. Structure, orientation and affinity for interfaces and lipids of ideally amphipathic lytic $LiK_j(i{=}2j)$ peptides. *Biochim. Biophys. Acta.* 1416:176–194.

36. Labourdenne, S., N. Gaudry-Rolland, …, C. Rivière. 1994. The oil-drop tensiometer: potential applications for studying the kinetics of (phospho)lipase action. *Chem. Phys. Lipids.* 71:163–173.

37. Lucassen-Reynders, E. H., A. Cagna, and J. Lucassen. 2001. Gibbs elasticity, surface dilational modulus and diffusional relaxation in nonionic surfactant monolayers. *Colloids Surf. A Physicochem. Eng. Asp.* 186:63–72.

38. Benjamins, J., J. Lyklema, and E. H. Lucassen-Reynders. 2006. Compression/expansion rheology of oil/water interfaces with adsorbed proteins. Comparison with the air/water surface. *Langmuir.* 22:6181–6188.

39. Diamond, R. 1974. Real-space refinement of the structure of hen egg-white lysozyme. *J. Mol. Biol.* 82:371–391.

40. Pasquini, C. 2003. Near infrared spectroscopy: fundamentals, practical aspects and analytical applications. *J. Braz. Chem. Soc.* 14:198–219.

41. Barth, A. 2007. Infrared spectroscopy of proteins. *Biochim. Biophys. Acta.* 1767:1073–1101.

42. Desfougères, Y., A. Saint-Jalmes, …, F. Nau. 2011. Strong improvement of interfacial properties can result from slight structural modifications of proteins: the case of native and dry-heated lysozyme. *Langmuir.* 27:14947–14957.

43. Mitsche, M. A., L. Wang, and D. M. Small. 2010. Adsorption of egg phosphatidylcholine to an air/water and triolein/water bubble interface: use of the 2-dimensional phase rule to estimate the surface composition of a phospholipid/triolein/water surface as a function of surface pressure. *J. Phys. Chem. B.* 114:3276–3284.

44. de La Fournière, L., M. G. Ivanova, …, R. Verger. 1994. Surface behaviour of human pancreatic and gastric lipases. *Colloids Surf. B Biointerfaces.* 2:585–593.

45. Boisselier, É., P. Calvez, …, C. Salesse. 2012. Influence of the physical state of phospholipid monolayers on protein binding. *Langmuir.* 28: 9680–9688.

46. Mudgil, P., M. Torres, and T. J. Millar. 2006. Adsorption of lysozyme to phospholipid and Meibomian lipid monolayer films. *Colloids Surf. B Biointerfaces.* 48:128–137.

47. D'Urzo, A., A. Konijnenberg, …, R. Grandori. 2015. Molecular basis for structural heterogeneity of an intrinsically disordered protein bound to a partner by combined ESI-IM-MS and modeling. *J. Am. Soc. Mass Spectrom.* 26:472–481.

48. Ta, H. P., K. Berthelot, …, S. Lecomte. 2011. Comparative studies of nontoxic and toxic amyloids interacting with membrane models at the air-water interface. *Langmuir.* 27:4797–4807.

49. Lad, M. D., F. Birembaut, …, R. J. Green. 2006. The adsorbed conformation of globular proteins at the air/water interface. *Phys. Chem. Chem. Phys.* 8:2179–2186.

50. Postel, C., O. Abillon, and B. Desbat. 2003. Structure and denaturation of adsorbed lysozyme at the air-water interface. *J. Colloid Interface Sci.* 266:74–81.

51. Malcolm, A. S., A. F. Dexter, and A. P. Middelberg. 2006. Mechanical properties of interfacial films formed by lysozyme self-assembly at the air-water interface. *Langmuir.* 22:8897–8905.

52. Lu, J. R., T. J. Su, …, R. Cubitt. 1998. The denaturation of lysozyme layers adsorbed at the hydrophobic solid/liquid surface studied by neutron reflection. *J. Colloid Interface Sci.* 206:212–223.

53. Su, T. J., J. R. Lu, …, J. Penfold. 1998. The adsorption of lysozyme at the silica-water interface: a neutron reflection study. *J. Colloid Interface Sci.* 203:419–429.

54. Conde, M. M., O. Conde, …, J. Miñones, Jr. 2011. How to obtain a well-spread monolayer of lysozyme at the air/water interfaces. *J. Colloid Interface Sci.* 361:351–360.

55. Sethuraman, A., G. Vedantham, …, G. Belfort. 2004. Protein unfolding at interfaces: slow dynamics of α-helix to β-sheet transition. *Proteins.* 56:669–678.

56. Gorbenko, G. P., V. M. Ioffe, and P. K. Kinnunen. 2007. Binding of lysozyme to phospholipid bilayers: evidence for protein aggregation upon membrane association. *Biophys. J.* 93:140–153.

57. Dorosz, J., R. Volinsky, …, R. Jelinek. 2009. Phospholipid-induced fibrillation of a prion amyloidogenic determinant at the air/water interface. *Langmuir.* 25:12501–12506.

58. López-Montero, I., P. López-Navajas, …, F. Monroy. 2013. Intrinsic disorder of the bacterial cell division protein ZipA: coil-to-brush conformational transition. *FASEB J.* 27:3363–3375.

59. Toto, A., C. Camilloni, …, S. Gianni. 2016. Molecular recognition by templated folding of an intrinsically disordered protein. *Sci. Rep.* 6:21994.

60. Scheuble, N., M. Lussi, …, P. Fischer. 2016. Blocking gastric lipase adsorption and displacement processes with viscoelastic biopolymer adsorption layers. *Biomacromolecules.* 17:3328–3337.

61. Sinthuvanich, C., A. S. Veiga, …, J. P. Schneider. 2012. Anti-cancer β-hairpin peptides: membrane-induced folding triggers activity. *J. Am. Chem. Soc.* 134:6210–6217.

62. Ozenne, V., F. Bauer, …, M. Blackledge. 2012. Flexible-Meccano: a tool for the generation of explicit ensemble descriptions of intrinsically disordered proteins and their associated experimental observables. *Bioinformatics.* 28:1463–1470.

63. Erales, J., M. Beltrandi, …, S. Longhi. 2015. Insights into the Hendra virus NTAIL-XD complex: evidence for a parallel organization of the helical MoRE at the XD surface stabilized by a combination of hydrophobic and polar interactions. *Biochim. Biophys. Acta.* 1854:1038–1053.

64. DeLano, W. L. 2002. The PyMOL Molecular Graphics System. *Proteins Struct. Funct. Bioinformat.* 30:442–454.

65. Longhi, S., V. Receveur-Bréchot, …, B. Canard. 2003. The C-terminal domain of the measles virus nucleoprotein is intrinsically disordered and folds upon binding to the C-terminal moiety of the phosphoprotein. *J. Biol. Chem.* 278:18638–18648.